Optical Rheology of Biological Cells

Falk Wottawah,[1,2] Stefan Schinkinger,[1,2] Bryan Lincoln,[1,2] Revathi Ananthakrishnan,[1,2] Maren Romeyke,[1] Jochen Guck,[1] and Josef Käs[1]

[1]*Institute for Soft Matter Physics, University of Leipzig, Linnéstrasse 5, 04103 Leipzig, Germany*
[2]*Center for Nonlinear Dynamics, University of Texas at Austin, Austin, Texas 78712, USA*

(Received 6 August 2004; published 11 March 2005)

A step stress deforming suspended cells causes a passive relaxation, due to a transiently cross-linked isotropic actin cortex underlying the cellular membrane. The fluid-to-solid transition occurs at a relaxation time coinciding with unbinding times of actin cross-linking proteins. Elastic contributions from slowly relaxing entangled filaments are negligible. The symmetric geometry of suspended cells ensures minimal statistical variability in their viscoelastic properties in contrast with adherent cells and thus is defining for different cell types. Mechanical stimuli on time scales of minutes trigger active structural responses.

DOI: 10.1103/PhysRevLett.94.098103 PACS numbers: 87.16.Ka, 64.70.Dv, 83.85.Ei, 87.19.Rr

The cytoskeleton, an intracellular polymer network, is essential for cellular functions such as motility, organelle transport, mechanotransduction, and mitosis. It is a composite of three different types of polymers: flexible to semiflexible intermediate filaments, semiflexible actin filaments, and rigid microtubules. Its structural response is the basis for the mechanical properties of cells [1,2], exhibiting passive and active responses to deformations. Differences to conventional polymers can even be seen in their passive relaxation behavior. The inherent nature of these biopolymer networks with binding energies on the order of a few k_BT leads to a transience which impacts polymer relaxation.

Previous experiments aimed toward an understanding of the origin of cellular viscoelasticity have either focused on *in vitro* rheology of individual cytoskeletal constituents [3,4] or on measurements of cells characterized by a highly inhomogeneous asymmetric cytoskeletal architecture [5–7]. These *in vitro* experiments have not yet been able to investigate the cytoskeleton as a compound material with its full complexity. Previous measurements on cells showed a large variability in the obtained viscoelastic moduli caused by the inhomogeneity and anisotropy of the cytoskeleton of adhered cells, which make interpretation difficult.

The optical stretcher is well suited to perform cell rheology on a simple spherical cell geometry, bridging between data on cytoskeletal components and *in vivo* measurements of the cytoskeleton in a widely varying state [8]. A cell is stretched between two laser beams [see Fig. 1(a)]. The deformation is caused by an optically induced surface stress σ, which can be well approximated with $\sigma(\theta) = \sigma_0 \cos^n\theta$, where θ is the azimuthal angle relative to the laser axis. σ_0 is the peak stress along the laser axis [8]. In individual measurements the deforming peak stress is varied between $\sigma_0 = 7$–18 Pa using by a fiber laser ($\lambda = 1064$ nm, IPG Photonics). Cells are trapped at a low power of 200 mW/beam, which does not cause measurable deformation. Heating effects during stretching are ~ 1–$2K$ [9] and thus negligible. This is confirmed by an unaltered cytoskeleton, proliferation activity, and cell motility, as well as further cell viability tests [8,10]. A time dependent step stress $\sigma(t)$ is applied to a cell between $t = 0$ and t_1 and its resulting relative radial deformation (i.e., axial strain) given by $\gamma(t) = \frac{\Delta r(t)}{r}$, is observed, where r is the radius of the cell along the laser beam axis at trap power, and $\Delta r(t)$ is the resulting radial extension [Figs. 1(b)–1(d)].

From several investigated cell lines and primary cells, we have chosen NIH/3T3 and SV-T2 fibroblasts to exemplify the results typically found for suspended cells. Since SV-T2 cells have a reduced actin cytoskeleton with respect to NIH/3T3 cells, the two cell lines illustrate how cytoskeletal differences are reflected in our measurements. Cells were individually subjected to a step stress. To examine their mechanical response on different time scales, the duration of deforming stress was varied between tenths of a second and minutes. The resulting relative radial deformation was recorded using video microscopy at 30 frames/s. The deformation was analyzed with a custom image-analysis algorithm.

The time dependence of γ in response to a constant step stress and the consequential relaxation behavior are passive and viscoelastic when stretching for 0.2, 2, and 10 s [see Figs. 1(b)–1(d)]. The response, as shown for NIH/3T3 fibroblasts in Fig. 1, displays a steep increase in axial strain for the first 0.2 s of a stretch, followed by a reduced increase for 1–3 s, and ultimately reaches a plateau. After stress relaxation, cells remain at about 30%–60% of their maximum strain. To extract the viscoelastic stress-strain relation of the cell in the investigated linear regime, the following constitutive equation was used [11]:

$$a_1 \partial_t \gamma(t) + a_2 \partial_t^2 \gamma(t) = \sigma(t) + b_1 \partial_t \sigma(t). \qquad (1)$$

It captures the initial elastic, the subsequent viscous, and the final relaxation behavior. For the applied step stress it was sufficient to truncate the expansion of the stress after

the first-order derivative and of the strain after the second-order derivative. The zeroth-order term of the strain expansion is negligible, as the strain does not recover completely [12].

Solving (1) for $\sigma(t) = F_G\sigma_0\Theta(t)\Theta(t_1 - t)$ reveals the temporal development of the axial strain. The geometric factor F_G accounts for the specific deformation induced on a shell-like viscoelastic object [13]. We attribute the initial viscoelastic response to the actin cytoskeleton in agreement with previous qualitative observations [14]. The fluorescence pictures of the suspended cells (see the inset of Fig. 2) show a thick cortical actin layer underlying the plasma membrane, but no stress fibers, while in adhered cells the dominant element of the actin cytoskeleton are stress fibers [15]. The optically determined actin shell thickness was 15%–20% of the cells' radii depending on the cell type. The absolute value impacts only the magnitude of the measured elastic constants. The temporal development of the axial strain for $0 < t < t_1$then is

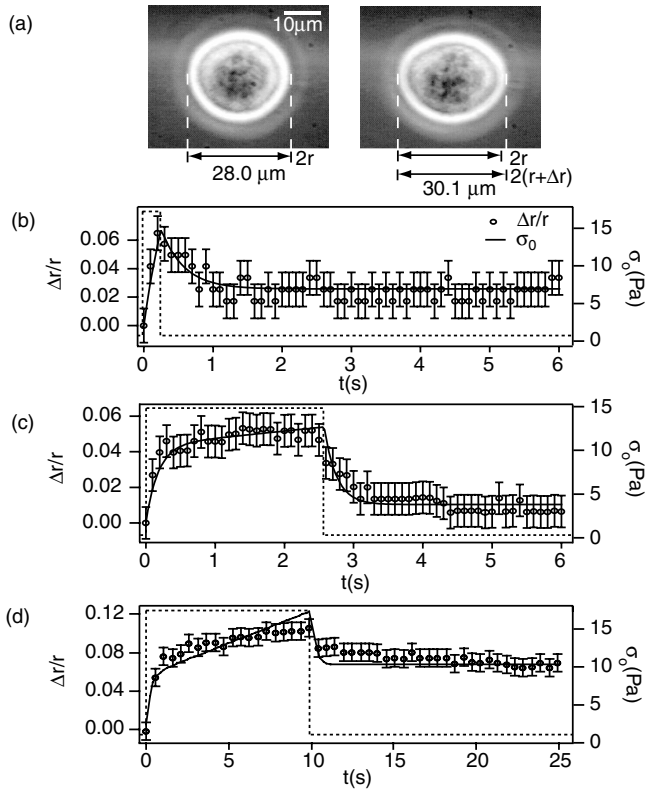

FIG. 1. An NIH/3T3 cell is trapped between two horizontally opposing, divergent laser beams. In a step stress experiment it is stretched as the laser power is increased and relaxes when the power is reduced. (a) Phase contrast images are used to analyze the radial deformation. (b)–(d) Development of axial strain $\gamma = \frac{\Delta r}{r}$ with time t when stretching an NIH/3T3 cell for 0.2 s (b), 2.5 s (c), and 10 s (d). Equations (2) and (3) were fitted to the data (solid lines).

$$\gamma(t) = F_G\sigma_0\left(\frac{b_1}{a_1} - \frac{a_2}{a_1^2}\right)(1 - e^{-(a_1/a_2)t}) + \frac{F_G\sigma_0}{a_1}t \quad (2)$$

and for $t > t_1$

$$\gamma(t) = F_G\sigma_0\left(\frac{b_1}{a_1} - \frac{a_2}{a_1^2}\right)(1 - e^{-(a_1/a_2)t_1})e^{-(a_1/a_2)(t-t_1)} + \frac{F_G\sigma_0}{a_1}t_1. \quad (3)$$

Equations (2) and (3) were fitted to the individually measured axial strain data of NIH/3T3 and SV-T2 cells, with a statistically significant sample size of 30 cells per cell type. These fits can be seen in Fig. 1. The strain can be described up to several seconds, but the fit for 10 s in Fig. 1(d) shows the limitation of the model for longer stretching times. Equation (2) becomes inappropriate since the strain reaches a plateau and further fluidlike extension is prevented by an elastic component, which now dominates the temporal deformation. This is consistent with the observation that the cell elastically relaxes up to 60% of the maximum deformation for 10 s stretches.

The fits allow the extraction of the parameters a_1, a_2, and b_1, which determine the viscoelastic constitutive equation of each individual cell. With $\gamma(t)$, the two components of the complex shear modulus $G^*(\omega)$, the storage modulus $G'(\omega)$, and loss modulus $G''(\omega)$ are obtained for single cells [11], where ω is the deforming frequency:

$$G'(\omega) = \frac{1}{2(1+\mu)}\left(\frac{\omega^2(a_1b_1 - a_2)}{1 + \omega^2 b_1^2}\right), \quad (4)$$

$$G''(\omega) = \frac{1}{2(1+\mu)}\left(\frac{\omega a_1 + \omega^3 a_2 b_1}{1 + \omega^2 b_1^2}\right). \quad (5)$$

A graph of $G'(\omega)$ and $G''(\omega)$ for a single suspended NIH/3T3 fibroblast is shown in Fig. 2 [16]. The cell displays an elastic plateau and a fluid-to-solid transition in the studied time and frequency regime. For an isotropic actin network as the dominating viscoelastic element, an elastic plateau was to be expected from *in vitro* rheology on entangled and cross-linked actin networks [3,4] as well as from atomic force microscopy measurements probing the actin cortex and avoiding stress fibers [7].

The average plateau moduli were $G'_{\mathrm{NIH/3T3}} = 100 \pm 10$ Pa and $G'_{\mathrm{SV\text{-}T2}} = 63 \pm 7$ Pa. For a statistical error of 10% (standard error of mean), a sample size of 30 cells was sufficient. Student's t test clearly identifies the existence of two separate populations (confidence $\geq$ 99.9%). Narrow statistical distributions of shear moduli which distinguish different cell populations with samples of less than 100 cells were also found for other cell lines, such as breast epithelial cell lines, white blood cells, primary and immortal keratinocytes, and adult stem cells. The unexpectedly low variance in the measurement of a cell type's viscoelastic constants (this does not solely apply

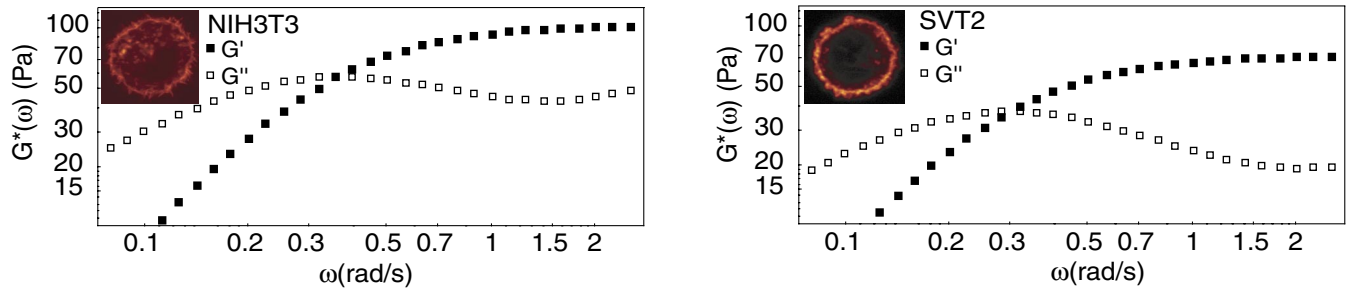

FIG. 2 (color). Storage $G'(\omega)$ and loss modulus $G''(\omega)$ for an NIH/3T3 fibroblast (left) and an SV-T2 fibroblast (right). The insets display the differences in actin distribution and concentration between NIH/3T3 and SV-T2 cells fluorescently labeled with TRITC-Phalloidin at a concentration of 3 μg/ml.

to the plateau modulus) contrasts to the large range of elastic constants obtained with other techniques. The controlled deformation of the whole cell, the symmetry of the suspended cells, and the absence of stress fibers generate a defined and consistent state for the measured cells.

Since SV-T2 cells possess $\approx 50\%$ less F-actin measured by laser scanning cytometry (data not shown), their lower plateau modulus is conceivable. In fibroblasts, a typical concentration of actin filaments is 10 mg/ml [17,18] with a filament length of about 1 μm [14], which puts these networks in the tightly entangled regime [2]. Using these parameters, a minute value of $G' \approx 5$ Pa is calculated for an entangled actin solution [2], while for a permanently cross-linked actin solution the plateau modulus is calculated to be $G' \approx 680$ Pa [1]. These estimates demonstrate that only cross-linked actin filaments contribute significantly to the elastic strength of a cell. Since the elastic strength of the actin cortex depends not only on the amount of actin, but also on the shell thickness and cross-linking protein concentration, a direct estimate of the decreased plateau modulus in SV-T2 cells with respect to NIH/3T3 cells is not possible.

We also expect that the intermediate filament vimentin does not significantly contribute to the linear elastic strength of fibroblasts. Vimentin has a persistence length of $l_p \approx 1$ μm and an intracellular concentration $\rho \approx 2.5 \times 10^{-2}$ mg/ml [19,20]. Assuming a tightly entangled network, this amounts to a negligible elastic strength on the order of $G' \approx 10^{-5}$ Pa [1]. Microtubules emanate from the microtubule organizing center near the nucleus toward the cell membrane, and thus conventional polymer theories do not apply for this complex architecture.

For the investigated cells—independent of the height of the plateau modulus—the elastic plateau ($G' > G''$) ends for $\omega \leq 0.6$ rad/s. The consequential fluid-to-solid transition is characterized by a terminal relaxation time $\tau_t = 2.8 \pm 0.5$ s. Since intermediate filaments are quasipermanently cross-linked, and the scaffold of microtubules remains unchanged on time scales longer than tens of seconds, we can rule out these two cytoskeletal elements as the origin of the observed dynamic behavior. Still, these two cytoskeletal elements may contribute to the elastic response for long deformations (≥ 10 s). The finding that in the linear regime the initial viscoelastic behavior is caused by the actin cortex and that the latter elastic behavior originates from the microtubules and intermediate filaments is consistent with changes of the viscoelastic behavior observed when cytoskeletal disrupting agents (Latrunculin A for actin; nocodazole for microtubules) are added (data not shown).

The actin cytoskeleton remains as the cause of the fluid-to-solid transition. Entangled actin filaments can be ruled out as the origin of the transition. The reptation time of actin filaments of 1 μm length in a cell's cytoplasm is $\tau_r \approx 400$ s ($\eta = 130$ Pa s) [21,22], which exceeds the observed relaxation time. Despite this long relaxation, causing the entangled filaments to behave gel-like on time scales beyond the terminal transition time measured, their contribution can be omitted as their elastic strength is negligible. This counterintuitively means that the cross-linked fraction causes the fluid-to-elastic transition.

The amount of cross-linked filaments is determined by the cross-linking proteins present in fibroblasts, predomi-

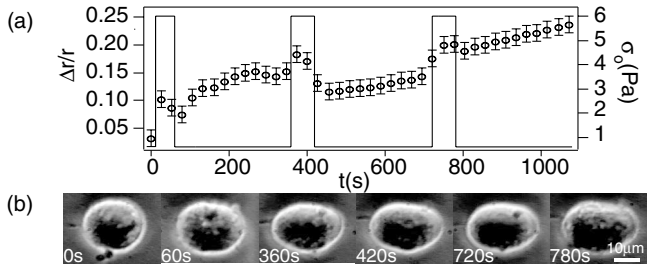

FIG. 3. An NIH/3T3 cell is stretched for 60 s with $\sigma_0 = 6$ Pa and given a 5 min relaxation phase, during which minimal trapping forces are applied. This process is repeated 3 times. (a) Even at low trap powers, where the optical surface stress is too small to stretch the cell, active extension along the laser axis is observed. (b) Phase contrast images of the temporal development of the elongating cell studied in (a).

nantly α-actinin, filamin, and Arp 2/3 [23–25]. These proteins not only affect the network's static but also its dynamic properties, because they transiently bind to actin filaments. Typical binding times are in the range of 0.2–3 s [23,24,26]. This allows cross-linked actin networks to form a unique hybrid between an elastic gel on time scales shorter than the binding times and a fluid on longer times.

It was not possible to evaluate our rheological data within the framework of a recently observed power law behavior [6,27,28]. This difference could be attributed to a suspended cell's different cytoskeletal architecture with respect to adherent cells. The investigated cells do not show the complexity of being a compound material of an isotropic actin mesh and stress fibers. Such power law behavior might stem from the influence of contractile elements, such as actin stress fibers [28,29].

For the role of actin networks in a cell, our results verify that only cross-linked filaments attribute to the mechanical strength. This is consistent with the loss of structural integrity in cells lacking actin cross-linking proteins [30]. This dominance of cross-linked filaments results in novel polymer dynamics since the terminal relaxation time is determined by the dissociation dynamics of the cross-linking proteins. Thus, intracellular actin networks provide only transient support, requiring active responses and restructuring of the actin cytoskeleton to assure long term mechanical integrity of a cell.

Apart from passive viscoelastic responses to stress shown for the 0.2, 2, and 10 s stretches, reactions of cells differ drastically when subjected to stress for a time period of about 1 min. Figure 3 shows an NIH/3T3 fibroblast being stretched for 60 s, with a subsequent relaxation phase of 5 min. During the relaxation phase, the cell is held in the trap at a low laser power, which is insufficient to stretch the cell. Cellular extension is not only observed when significant stress is applied, but the cell continues to extend along the axis during the relaxation phase. This can be understood only as an active response of the cytoskeleton to mechanical stimuli. The monitored fluidlike extension during the relaxation phase requires extending forces in the range of 10–1000 pN. They can be estimated under the assumption of a linear viscous extension during the relaxation phases and the knowledge of the cellular viscosity. These forces exceed any possible contribution of external trapping forces suggesting internal cellular processes cause the extension. Such self-propelled active and dynamic restructuring is a necessity for active cellular function.

Our study identifies suspended cells as well-defined viscoelastic objects. The small variability in the results has to be attributed to a tightly controlled and regulated cytoskeleton. This makes suspended cells ideal to distinguish cells based on their cytoskeletal characteristics. We find the actin cortex responsible for the initial viscoelastic response. Transiently cross-linked actin filaments solely contribute to this response. Consequentially, the stress relaxation behavior is determined by the binding dynamics of actin cross-linking proteins. This intermediate between a fluid and an elastic gel is perfectly suited for the highly adaptive, active structural role of the cytoskeleton.

This work was supported by the Alexander von Humboldt Foundation.

[1] F. C. MacKintosh, J. Käs, and P. A. Janmey, Phys. Rev. Lett. **75**, 4425 (1995).
[2] D. Morse, Macromolecules **31**, 7030 (1998); **31**, 7044 (1998).
[3] B. Hinner *et al.*, Phys. Rev. Lett. **81**, 2614 (1998).
[4] M. L. Gardel *et al.*, Science **304**, 1301 (2004).
[5] J. C. Crocker *et al.*, Phys. Rev. Lett. **85**, 888 (2000).
[6] B. Fabry *et al.*, Phys. Rev. Lett. **87**, 148102 (2001).
[7] R. Mahaffy *et al.*, Biophys. J. **86**, 1777 (2004).
[8] J. Guck *et al.*, Biophys. J. **81**, 767 (2001).
[9] E. J. G. Peterman, F. Gittes, and C. F. Schmidt, Biophys. J. **84**, 1308 (2003).
[10] K. C. Neuman *et al.*, Biophys. J. **77**, 2856 (1999).
[11] S. W. Park and R. Schapery, Int. J. Solids Struct. **36**, 1653 (1999).
[12] The sensitivity of constitutive equation (1) to various viscoelastic responses was tested with objects showing different complex fluid behaviors; e.g., other terms have to be considered to explain the behavior of lipid vesicles in the optical stretcher compared to polymerosomes.
[13] A. I. Lure, *Three-Dimensional Problems of the Theory of Elasticity* (Interscience Publishers, New York, 1964).
[14] T. P. Stossel, J. Cell Biol. **99**, 15s (1984).
[15] A cell's state in a tissue matrix is in between these two extreme states of strongly adhered and not adhered cells, showing a cortical actin layer as well as a sparse distribution of stress fibers.
[16] A Poisson ratio of $\mu = 0.45$ is typical for these cells [7].
[17] K. Nagamalleswari and D. Safer, Mol. Cell. Biochem. **209**, 63 (2000).
[18] L. P. Cramer, L. J. Briggs, and H. R. Dawe, Cell Motil. Cytoskeleton **51**, 27 (2002).
[19] N. Mücke *et al.*, J. Mol. Biol. **335**, 1241 (2004).
[20] T. R. Coleman and E. Lazarides, J. Cell Sci. **103**, 689 (1992).
[21] A. Spiros and L. Edelstein-Keshet, Bull. Math. Biol. **60**, 275 (1998).
[22] J. Käs *et al.*, Biophys. J. **70**, 609 (1996).
[23] W. H. Goldmann and G. Isenberg, FEBS Lett. **336**, 408 (1993).
[24] R. D. Mullins, J. A. Heuser, and T. D. Pollard, Proc. Natl. Acad. Sci. U.S.A. **95**, 6181 (1998).
[25] L. Eichinger *et al.*, Biophys. J. **70**, 1054 (1996).
[26] D. H. Wachsstock, W. H. Schwarz, and T. D. Pollard, Biophys. J. **66**, 801 (1994).
[27] M. Balland, A. Richert, and F. Gallet, Eur. Biophys J. (to be published).
[28] G. Lenormand *et al.*, J. R. Soc. (London), Interface **1**, 91 (2004).
[29] P. Sollich, Phys. Rev. E **58**, 738 (1998).
[30] C. C. Cunningham *et al.*, Science **255**, 325 (1992).